

# Particle vibrational coupling in covariant density functional theory. \*

P. Ring<sup>1,†</sup> and E. Litvinova<sup>2,3,4,‡</sup>

<sup>1</sup>*Physik-Department der Technischen Universität München, D-85748 Garching, Germany*

<sup>2</sup>*GSI Helmholtzzentrum für Schwerionenforschung, 64291 Darmstadt, Germany*

<sup>3</sup>*Frankfurt Institute for Advanced Studies,*

*Universität Frankfurt, 60438 Frankfurt am Main, Germany*

<sup>4</sup>*Institute of Physics and Power Engineering, 249033 Obninsk, Russia*

(Dated: October 11, 2018)

A consistent combination of covariant density functional theory (CDFT) and Landau-Migdal Theory of Finite Fermi Systems (TFFS) is presented. Both methods are in principle exact, but Landau-Migdal theory cannot describe ground state properties and density functional theory does not take into account the energy dependence of the self-energy and therefore fails to yield proper single-particle spectra as well as the coupling to complex configurations in the width of giant resonances. Starting from an energy functional, phonons and their vertices are calculated without any further parameters. They form the basis of particle-vibrational coupling leading to an energy dependence of the self-energy and an induced energy-dependent interaction in the response equation. A subtraction procedure avoids double counting. Applications in doubly magic nuclei and in a chain of superfluid nuclei show excellent agreement with experimental data.

## I. INTRODUCTION

The understanding of the structure of nuclei far from stability with extreme isospin is one the most exciting challenges of present nuclear physics. New experimental facilities with radioactive nuclear beams make it possible to investigate the nuclear chart to the very limits of nuclear binding. A wealth of structure phenomena in exotic nuclei have been reported and the next generation of radioactive-beam facilities will present new exciting opportunities to study not only the ground states but also excitations and spectra of these strongly interacting many-body systems. This situation has stimulated considerable new efforts on the theoretical side to understand the dynamics of the nuclear many-body problem by microscopic methods. Exact solutions of the non-relativistic

---

\* This article is dedicated to Prof. Spartak Belyaev on the occasion of his 85<sup>th</sup> birthday

<sup>†</sup>Electronic address: ring@ph.tum.de

<sup>‡</sup>Electronic address: litvinova@gsi.de

Schrödinger equation based on the bare nucleon-nucleon interaction are used to study very light nuclei with  $A \leq 12$  by an “ab initio” approach, modern shell-model calculations based on large scale diagonalization techniques and truncation schemes show considerable success in situations where configuration mixing calculations are possible, i.e. in light nuclei or in nuclei with single magic or doubly magic configurations. For the large majority of nuclei, however, a quantitative microscopic description is, so far, only possible by density functional theory (DFT) and its extensions. Although DFT can, in principle, provide an exact description of many-body problems[1], if the exact density functional is known, in nuclear physics one is far from a microscopic derivation of this functional. In addition, nuclei are self-bound systems. As a consequence of translational invariance the density in the laboratory frame is constant in space. Density functional theory in nuclei is therefore based on the intrinsic density, a concept that requires additional approximations [2, 3]. The most successful schemes of DFT in nuclei use a phenomenological ansatz incorporating as many symmetries of the system as possible and adjusting the parameters of the functional to ground state properties of a few characteristic nuclei on the nuclear chart. Considerable progress has been reported recently in constructing such functionals. For a recent review see [4].

One of the underlying symmetries of QCD is Lorentz invariance and therefore covariant density functionals [5, 6] are of particular interest in nuclear physics. This symmetry not only allows to describe the spin-orbit coupling, which has an essential influence on the underlying shell structure, in a consistent way, but it also puts stringent restrictions on the number of parameters in the corresponding functionals without reducing the quality of the agreement with experimental data.

Most of the nuclei are superfluid systems and therefore the inclusion of pairing correlations is essential for a correct description of structure phenomena in open-shell nuclei [7, 8]. Hartree-Bogoliubov theory provides a unified description of  $ph$ - and  $pp$ -correlations on a mean-field level by using two type of densities, the normal density matrix  $\hat{\rho} = \langle a^\dagger a \rangle$  and antisymmetric pairing tensor  $\hat{\kappa} = \langle aa \rangle$  [9]. According to Valatin these two densities can be combined to the generalized density matrix  $\hat{\mathcal{R}}$  of double dimension [10]. CDFT theory for superfluid systems is therefore based on a generalized Relativistic Hartree-Bogoliubov (RHB) energy density  $E_{RHB}[\hat{\mathcal{R}}]$ . The same is true for the Landau-Migdal theory and for all the methods discussed in this paper. For simplicity, however, we restrict all our considerations in this article to the case without pairing correlations. Pairing correlations can be included on all steps by using super-matrices. Details are given in Ref. [11]. Only in the applications we present also calculations in isotopic chains of open shell nuclei, that include pairing correlations.

A very successful example of a covariant density functional theory is the Relativistic Hartree-

Bogoliubov model [12]. It combines a density dependence through a non-linear coupling between the meson fields [13] with pairing correlations based on an effective interaction of finite range. A large variety of nuclear phenomena have been described over the years within this model: the equation of state in symmetric and asymmetric nuclear matter, ground state properties of finite spherical and deformed nuclei all over the periodic table [14] from light nuclei [15] to super-heavy elements [16], from the neutron drip line, where halo phenomena are observed [17] to the proton drip line [18] with nuclei unstable against the emission of protons [19].

In principle density functional theory can be used for the description of all properties depending on the single-particle density. It is therefore not only limited to the description of the ground state properties. The same density functionals have also been applied for a very successful description of excited states, such as rotational bands in normal and super-deformed nuclei [20, 21] and collective vibrations [22]. Rotations are treated in the cranking approximation providing a quasi-static description of the nuclear dynamics in a rotating frame and for the description of vibrations a time-dependent mean field approximation is used by assuming independent particle motion in time-dependent average fields [23]. In the small amplitude limit one obtains the relativistic Random Phase Approximation (RRPA) [24] and in superfluid nuclei the relativistic Quasiparticle Random Phase Approximation (RQRPA) [25]. This method provides a natural framework to investigate collective and non-collective excitations of  $ph$ - (or  $2qp$ ) character. It is successful in particular for the understanding of the position of giant resonances and spin- or/and isospin-excitations as the Gamov Teller Resonance (GTR) or the Isobaric Analog Resonance (IAR). Recently it has been also used for a theoretical interpretation of low lying E1-strengths observed in neutron rich isotopes (pygmy modes) [25] and for low-lying collective quadrupole excitations [26].

Density functional theory in nuclei is based on intrinsic densities and on the mean field approach. Therefore it cannot provide an exact treatment of the full nuclear dynamics. It breaks down in transitional nuclei, where the intrinsic density is not well defined and where one has to include correlations going beyond the mean field approximation by treating quantum fluctuations through a superposition of several mean field solutions, as for instance in the Generator Coordinate Method (GCM) [9]. But it also provides a poor approximation for the single-particle spectra particularly in ideal shell model nuclei such as  $^{208}\text{Pb}$  with closed protons and neutron shells. One finds in self-consistent mean field calculations usually a considerably enhanced Hartree-Fock gap in the single-particle spectrum and a reduced level density at the Fermi surface as compared with the experiment. It is well known that this fact is connected with the relatively small effective mass in such models. Mahaux and collaborators [27] have shown that the effective mass in nuclear

matter is roughly  $m^*/m \approx 0.8$ . In finite nuclei it should be modified by the coupling of the single-particle motion to low-lying collective surface vibrations. This leads, in the vicinity of the Fermi surface, to an enhancement of  $m^*/m \approx 1$ . Non-self-consistent models with the bare mass ( $m^*/m \approx 1$ ) show indeed a single-particle spectrum with a level density close to the experiment. With a few exceptions, where the quadrupole motion has been studied within the relativistic Generator Coordinate Method (GCM) [28, 29], applications of covariant density functional theory to the description of excited states are limited to relativistic RPA, i.e. to configurations of  $1p1h$ -nature. None of these methods, however, can be applied to the investigation of the coupling to more complicated configurations, as it occurs for instance in the damping phenomena causing the width of giant resonances.

Already before density functional theory has been introduced in the sixties for the description of quantum mechanical many-body problems by Kohn and Sham [1] Landau has developed in the fifties his Fermi Liquid Theory (FLT) [30] for infinite systems. It has been extended to the Theory of Finite Fermi Systems (TFFS) [31] by Migdal. This theory provides another very successful method for the description of low-lying nuclear excitations [32]. It has several general properties in common with density functional theory. First, both theories are known to be exact, at least in principle, but in practice, in nuclear physics, the parameters entering these theories have to be determined in a phenomenological way by adjustment to experimental data. Second, both theories are based on a single-particle concept. DFT uses the mean field concept with Slater determinants in an effective single-particle potential as a vehicle to introduce shell-effects in the exact density functional introduced by Hohenberg and Kohn [33]. Fermi liquid theory is based on the concept of quasi-particles obeying a Dyson equation, which are defined as the basic excitations of the neighboring system with odd particle number. Third, in practical applications both theories describe in the simplest versions the nuclear excitations in the RPA approximation, i.e. by a linear combination of  $ph$ -configurations in an average nuclear potential.

However, there are also essential differences between these two concepts. First, in contrast to DFT, TFFS does not attempt to calculate the ground state properties of the many-body system, but it describes the nuclear excitations in terms of Landau quasi-particles and their interaction. Therefore the experimental data used to fix the phenomenological parameters of the theories are bulk properties of the ground state in the case of density functional theory, and properties of single-particle excitations and of the collective excitations in the case of finite Fermi systems theory. Second, in DFT the mean field is determined in a self-consistent way and therefore the RPA spectrum contains Goldstone modes at zero energy. This is usually not the case in TFFS calcula-

tions, which are based on a non-relativistic shell-model potential, whose parameters are adjusted to the experimental single-particle spectra. Therefore, apart from a few approximate attempts to treat the Goldstone modes by adjusting additional parameters in the effective quasiparticle interaction, there is no self-consistency in the RPA calculations of TFFS and the Goldstone modes do not separate from the other modes. They are distributed among the low-lying excitations. Third, modern versions of TFFS go much beyond the mean field approximation. The coupling between the particles and the phonons is investigated with Green's function techniques. Based on the phonons calculated in the framework of the RPA one has included particle-phonon coupling vertices and an energy dependence of the self-energy in the Dyson equation [34, 35]. This leads also to an induced interaction in the Bethe-Salpeter equation caused by the exchange of phonons which also depends on the energy. The coupling of particles and phonons has also been derived from Nuclear Field Theory (NFT) and its extensions [36–38]. Many aspects of the coupling between the quasi-particles and the collective vibrations have been investigated with these techniques [39–48] as well as with other kinds of approaches beyond RPA [49, 50] over the years.

We give here an overview over recent attempts [11, 51–53] to find a combination of the basic ideas of covariant density functional theory and Landau-Migdal theory and show as examples corresponding applications. The concept is similar to earlier work in Refs. [54–56], where specific non-relativistic energy functionals have been used to construct a Self-Consistent Theory of Finite Fermi Systems. The starting point is a covariant density functional  $E[\rho]$  widely used in the literature. It is adjusted to ground state properties of characteristic nuclei and, without any additional parameter, it provides the necessary input of finite Fermi systems theory, such as the mean field and the single-particle spectrum as well as an effective interaction between the  $ph$ -configurations in terms of the second derivative of the same energy  $E[\rho]$  with respect to the density. Thus the phenomenological input of Landau-Migdal theory is replaced by the results of density functional theory. The same interaction is used to calculate the vertices for particle-vibration coupling [51]. In a second step techniques of Landau-Migdal theory and its modern extensions are used to describe the coupling of one- and two-quasiparticle configurations. The main assumption of the quasiparticle-phonon coupling model is that two types of elementary excitations – two-quasiparticle and vibrational modes – are coupled in such a way that configurations of  $1p1h \otimes \text{phonon}$  type with low-lying phonons strongly compete with simple  $1p1h$  configurations close in energy or, in other words, that quasiparticles can emit and absorb phonons with rather high probabilities. In this way a fully consistent description of the many-body dynamics is obtained. As a result an induced additional interaction between single-particle and vibrational excitations provides a strong frag-

mentation of the pure RQRPA states causing the spreading width of giant resonances and the redistribution of the pygmy strength.

Two essential approximations are used in this context: First, the *Time-Blocking Approximation* (TBA) [44], that has been extended to systems with pairing correlations (QTBA) in Ref. [11], blocks in a special time-projection technique the  $1p1h$ -propagation through states which have a more complex structure than  $1p1h \otimes \text{phonon}$ . The nuclear response can then be explicitly calculated on the  $1p1h + 1p1h \otimes \text{phonon}$  level by summation of an infinite series of Feynman's diagrams. Second, a special *subtraction technique* guarantees, that there is no double counting between the additional correlations introduced by particle-vibration coupling and the ground state correlations already taken into account in the phenomenological density functional. These two tools are essential for the success of this method. TBA introduces a consistent truncation scheme into the Bethe-Salpeter equation and without it it would be hard to solve the equations explicitly. The subtraction method is the essential tool to connect density functional theory so far used only on the level of mean field theory, i.e. on the RPA level, with the extended Landau-Migdal theory, where complex configurations are included through particle-vibration coupling.

The structure of the paper is the following: In Section II we discuss shortly the general formalism of covariant density functional theory, we introduce in Section III the concept of the energy-dependent self-energy  $\Sigma(\varepsilon)$  and the vertices of particle-vibration coupling in the relativistic framework, and we discuss in Section IV the response formalism, the time blocking approximation and the subtraction mechanism for the response function. In Section V we present recent numerical applications for the calculation of level densities at the Fermi surface and the spreading width of the several nuclei. Section VI contains a brief summary and an outlook for future applications.

## II. THE RELATIVISTIC ENERGY DENSITY FUNCTIONAL

Covariant density functional theory uses the Walecka model [57] as a Lorentz invariant framework for the formulation of the density functional. In this model the nucleus is described as a system of Dirac nucleons coupled to the exchange mesons and the electromagnetic field through an effective Lagrangian. The isoscalar scalar  $\sigma$ -meson, the isoscalar vector  $\omega$ -meson, and the isovector vector  $\rho$ -meson build the minimal set of meson fields that together with the electromagnetic field is necessary for a quantitative description of bulk and single-particle nuclear properties [5, 57–60]. The model is defined by the Lagrangian density

$$\mathcal{L} = \mathcal{L}_N + \mathcal{L}_m + \mathcal{L}_{int}. \quad (1)$$

$\mathcal{L}_N$  denotes the Lagrangian of the free nucleon

$$\mathcal{L}_N = \bar{\psi} (i\gamma^\mu \partial_\mu - m) \psi, \quad (2)$$

where  $m$  is the bare nucleon mass and  $\psi$  denotes the Dirac spinor.  $\mathcal{L}_m$  is the Lagrangian of the free meson fields and the electromagnetic field

$$\begin{aligned} \mathcal{L}_m = & \frac{1}{2} \partial_\mu \sigma \partial^\mu \sigma - \frac{1}{2} m_\sigma^2 \sigma^2 - \frac{1}{4} \Omega_{\mu\nu} \Omega^{\mu\nu} + \frac{1}{2} m_\omega^2 \omega_\mu \omega^\mu \\ & - \frac{1}{4} \vec{R}_{\mu\nu} \vec{R}^{\mu\nu} + \frac{1}{2} m_\rho^2 \vec{\rho}_\mu \vec{\rho}^\mu - \frac{1}{4} F_{\mu\nu} F^{\mu\nu}, \end{aligned} \quad (3)$$

with the corresponding masses  $m_\sigma$ ,  $m_\omega$ ,  $m_\rho$ , and  $\Omega_{\mu\nu}$ ,  $\vec{R}_{\mu\nu}$ ,  $F_{\mu\nu}$  are field tensors (arrows denote isovectors and boldface symbols are for vectors in ordinary space). The minimal set of interaction terms is contained in  $\mathcal{L}_{int}$

$$\mathcal{L}_{int} = -\bar{\psi} \Gamma_\sigma \sigma \psi - \bar{\psi} \Gamma_\omega^\mu \omega_\mu \psi - \bar{\psi} \vec{\Gamma}_\rho^\mu \vec{\rho}_\mu \psi - \bar{\psi} \Gamma_e^\mu A_\mu \psi. \quad (4)$$

with the vertices

$$\Gamma_\sigma = g_\sigma, \quad \Gamma_\omega^\mu = g_\omega \gamma^\mu, \quad \vec{\Gamma}_\rho^\mu = g_\rho \vec{\tau} \gamma^\mu, \quad \Gamma_e^\mu = q \gamma^\mu, \quad (5)$$

with the coupling constants  $g_\sigma$ ,  $g_\omega$ ,  $g_\rho$  and  $q$  ( $e$  or 0 for protons or neutrons). Already in the earliest applications of the RMF framework it was realized, however, that this simple model with interaction terms only linear in the meson fields, does not provide a quantitative description of complex nuclear systems. An effective density dependence was introduced [13] by replacing the quadratic  $\sigma$ -potential  $\frac{1}{2} m_\sigma^2 \sigma^2$  with a non-linear meson coupling potential  $U(\sigma)$ , which contains additional parameters. This particular form of the non-linear potential has become standard in applications of RMF models, although additional non-linear interaction terms, both in the isoscalar and isovector channels, have also been considered [61–64].

From the model Lagrangian density the classical variation principle leads to the equations of motion:

$$[\gamma^\mu (i\partial_\mu + V_\mu) + m + S] \psi = 0. \quad (6)$$

If one neglects retardation effects for the meson fields, which is well justified because of the large meson masses, a self-consistent solution is obtained when the time-dependent mean-field potentials

$$S = g_\sigma \sigma, \quad V_\mu = g_\omega \omega_\mu + g_\rho \vec{\tau} \vec{\rho}_\mu + q A_\mu,$$

are calculated at each step in time by the solution of the static Klein-Gordon equations

$$-\Delta\phi_m + U'(\phi_m) = \pm \langle \bar{\psi} \Gamma_m \psi \rangle, \quad (7)$$

where the (+) sign is for vector fields and the (−) sign for the scalar field. The index  $m$  denotes mesons and the photon, i.e.  $\phi_m \equiv \{\sigma, \omega^\mu, \vec{\rho}^\mu, A^\mu\}$ , and  $U'(\phi_m)$  is derivative of the corresponding potential with respect to the meson field.

In applications to nuclear matter and finite nuclei, the relativistic models are used in the *no-sea* approximation, i.e. the Dirac sea of states with negative energies does not contribute to the densities and currents and one uses

$$\langle \bar{\psi} \Gamma_m \psi \rangle = \sum_{i=1}^A \bar{\psi}_i(\mathbf{r}, t) \Gamma_m \psi_i(\mathbf{r}, t), \quad (8)$$

where the sum runs only over the occupied states in the Fermi sea, i.e. vacuum polarization effects are neglected. In fact, many effects that go beyond the classical mean-field level are apparently neglected in these models: Fock terms, vacuum polarization effects, and the short range Brueckner-type correlations. The experimental data to which the meson-nucleon couplings are adjusted, however, contain all these effects and much more. It follows that effects beyond the mean-field level are implicitly included in the RMF approach by adjusting the model parameters to reproduce a selected empirical data set. Vacuum effects, chiral symmetry, nucleon substructure, exchange terms, long- and short-range correlation effects are, therefore, effectively included in this approach although neither of them can be accessed separately.

The set of coupled equations (6) and (7) define the relativistic mean field (RMF) model. In the stationary case they reduce to a nonlinear eigenvalue problem and in the time-dependent case they describe the nonlinear propagation of the Dirac spinors in time [23].

RMF models can be also formulated without explicitly including mesonic degrees of freedom. Meson-exchange interactions can be replaced by local four-point interactions between nucleons. It has been shown that the relativistic point-coupling models [65–67] are completely equivalent to the standard meson-exchange approach. In order to describe properties of finite nuclei on a quantitative level, the point-coupling models include also some higher order interaction terms. For instance, six-nucleon vertices  $(\bar{\psi}\psi)^3$ , and eight-nucleon vertices  $(\bar{\psi}\psi)^4$  and  $[(\bar{\psi}\gamma_\mu\psi)(\bar{\psi}\gamma^\mu\psi)]^2$ .

These relatively simple models turn out to provide a very successful phenomenological description of the nuclear many-body system all over the periodic table. Relatively few parameters are adjusted to ground state properties of a few finite nuclei. At a first glance it is not easy to see how can such a simple approach can be so successful. This can be only understood if one considers



that this model represents an approximate implementation of Kohn-Sham density functional theory (DFT)[1, 68, 69], which is successfully employed in the treatment of the quantum many-body problem in atomic, molecular and condensed matter physics.

It is evident that equations of motion (6) and (7) can also be directly derived from a density functional. Using the definition of the relativistic single-nucleon density matrix

$$\hat{\rho}(\mathbf{r}, \mathbf{r}', t) = \sum_{i=1}^A |\psi_i(\mathbf{r}, t)\rangle \langle \psi_i(\mathbf{r}', t)|, \quad (9)$$

the total energy can be written as a functional of the density matrix  $\hat{\rho}$  and of the meson fields

$$E_{RMF}[\hat{\rho}, \phi_m] = \text{Tr}[(\boldsymbol{\alpha}\mathbf{p} + \beta m)\hat{\rho}] \pm \int \left[ \frac{1}{2}(\nabla\phi_m)^2 + U(\phi_m) \right] d^3r + \text{Tr}[(\Gamma_m\phi_m)\hat{\rho}]. \quad (10)$$

The trace operation involves a sum over the Dirac indices and an integral in coordinate space. The index  $m$  is used as generic notation for all mesons and the photon.

### III. THE ENERGY DEPENDENCE OF THE SELF-ENERGY

In a relativistic many-body theory the motion of single nucleons in the nuclear medium is described by the Dyson equation

$$(\gamma^\mu P_\mu - m^*)|\psi\rangle = 0, \quad (11)$$

where the self-energy is given by

$$m^* = m + \Sigma_s \quad (12)$$

with the scalar part  $\Sigma_s$  of the self-energy and where the generalized four-vector momentum operator has the form

$$P_\mu = p_\mu - \Sigma_\mu = \left( i\frac{\partial}{\partial t} - \Sigma_0, i\nabla + \boldsymbol{\Sigma} \right) \quad (13)$$

with the vector part  $\Sigma^\mu$  of the self-energy

$$\Sigma^\mu = (\Sigma^0, \boldsymbol{\Sigma}). \quad (14)$$

The index 's' in the Eq. (12) denotes that the effective mass is described by the scalar  $\sigma$ -meson field. In order to characterize ground state properties the stationary Dirac equation has to be solved:

$$(\boldsymbol{\alpha}(\mathbf{p} - \boldsymbol{\Sigma}) + \beta m^* + \Sigma_0)|\psi\rangle = \varepsilon|\psi\rangle. \quad (15)$$

In the general case the full self-energy is non-local in space and also in time. This non-locality means that its Fourier transform has both momentum and energy dependence. We therefore decompose the total self-energy in a stationary local part and an energy-dependent non-local term:

$$\Sigma(\mathbf{r}, \mathbf{r}'; \omega) = \tilde{\Sigma}(\mathbf{r})\delta(\mathbf{r} - \mathbf{r}') + \Sigma^e(\mathbf{r}, \mathbf{r}'; \omega), \quad (16)$$

where all the components of the self-energy are involved:

$$\Sigma = (\Sigma_s, \Sigma_\mu), \quad \tilde{\Sigma} = (\tilde{\Sigma}_s, \tilde{\Sigma}_\mu), \quad \Sigma^e = (\Sigma_s^e, \Sigma_\mu^e)$$

and the index "e" indicates the energy dependence.

The energy-independent parts of the self-energy correspond to the average fields of the Walecka model:

$$\tilde{\Sigma}_s(\mathbf{r}) = S(\mathbf{r}), \quad \tilde{\Sigma}_\mu(\mathbf{r}) = V_\mu(\mathbf{r}) \quad (17)$$

These fields satisfy the inhomogeneous Klein-Gordon equations, where the sources are determined by the respective density and current distributions in a system of  $A$  nucleons.

We assume time-reversal symmetry that means the absence of currents in the nucleus and, thus, we find vanishing space-like components of  $\Sigma$ . The equation of the one-nucleon motion has the form:

$$(h_D + \beta\Sigma_s^e(\varepsilon) + \Sigma_0^e(\varepsilon))|\psi\rangle = \varepsilon|\psi\rangle \quad (18)$$

where  $h_D$  is the Dirac Hamiltonian

$$h_D = \boldsymbol{\alpha}\mathbf{p} + \beta(m + \tilde{\Sigma}_s) + \tilde{\Sigma}_0 \quad (19)$$

or, in the language of Green's functions

$$(\varepsilon - h_D - \beta\Sigma_s^e(\varepsilon) - \Sigma_0^e(\varepsilon))G(\varepsilon) = 1. \quad (20)$$

It turns out to be useful to work in the shell-model Dirac basis  $\{|\psi_k\rangle\}$  which diagonalizes the energy-independent part of the Dirac equation:

$$h_D|\psi_k\rangle = \varepsilon_k|\psi_k\rangle. \quad (21)$$

In this basis one can rewrite Eq. (20) as follows:

$$\sum_l \{(\varepsilon - \varepsilon_k)\delta_{kl} - \Sigma_{kl}^e(\varepsilon)\}G_{lk'}(\varepsilon) = \delta_{kk'}, \quad (22)$$

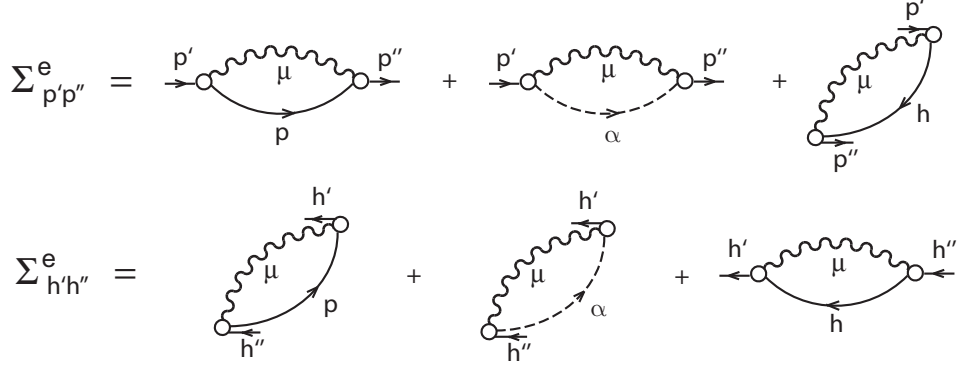


FIG. 1: The particle  $\Sigma_{p'p''}^e$  and the hole  $\Sigma_{h'h''}^e$  components of the relativistic self-energy in the graphical representation. Solid and dashed lines with arrows denote one-body propagators for particle ( $p$ ), hole ( $h$ ), and antiparticle ( $\alpha$ ) states. Wavy lines denote phonon ( $\mu$ ) propagators, empty circles are the particle-phonon coupling vertices  $\gamma^\mu$  in Eq. (25). The time direction is from the left to the right.

where the letter indices  $k, k', l$  denote full sets of the spherical quantum numbers.

Obviously, on this stage one needs some model assumptions. The particle-phonon coupling model [36] provides a rather simple approximation to describe the energy dependence of  $\Sigma^e(\varepsilon)$ . Within this model  $\Sigma^e(\varepsilon)$  is a convolution of the particle-phonon coupling amplitude  $\Gamma$  and the exact single-particle Green's function [70]:

$$\Sigma_{kl}^e(\varepsilon) = \sum_{k'l'} \int_{-\infty}^{+\infty} \frac{d\omega}{2\pi i} \Gamma_{kl'l'k'}(\omega) G_{k'l'}(\varepsilon + \omega), \quad (23)$$

where the amplitude

$$\Gamma_{kl'l'k'}(\omega) = - \sum_{\mu} \left( \frac{\gamma_{k'k}^{\mu*} \gamma_{l'l}^{\mu}}{\omega - \Omega^{\mu} + i\eta} - \frac{\gamma_{kk'}^{\mu} \gamma_{ll'}^{\mu*}}{\omega + \Omega^{\mu} - i\eta} \right) \quad (24)$$

is represented in terms of phonon vertexes  $\gamma^\mu$  and their frequencies  $\Omega^\mu$ . They are determined by the following relation:

$$\gamma_{kl}^{\mu} = \sum_{k'l'} \tilde{V}_{kl'l'k'} \delta \rho_{k'l'}. \quad (25)$$

$\delta \rho$  is the transition density and in the linearized version of the model  $\tilde{V}_{kl'l'k'}$  denotes the relativistic matrix element of the static residual interaction, i.e. the second derivative of the energy functional with respect to the density matrix

$$\tilde{V} = \frac{\delta^2 E_{RMF}[\hat{\rho}]}{\delta \hat{\rho} \delta \hat{\rho}} \quad (26)$$

In the linear approximation  $\delta\rho$  is not influenced by the particle-phonon coupling and can be computed within relativistic RPA or QRPA. The linearized version implies also that the energy-dependent part of the self-energy (23) contains the mean field Green's function  $\tilde{G}(\varepsilon) = (\varepsilon - h_D)^{-1}$  instead of the exact Green's function  $G$ . The graphical representation of the self-energy is given in Fig. 1. In contrast to the non-relativistic case, where one has occupied states below the Fermi surface (hole states  $h$ ) and empty states above the Fermi surface (particle states  $p$ ) we now have according to the no-sea approximation in addition empty states with negative energies in the Dirac sea (anti-particle states  $\alpha$ ). Particle and hole components are drawn assuming all the possible types of intermediate states.

Eq. (22) contains off-diagonal elements of the matrix  $\Sigma_{kl}^e$  with relatively large energy denominators. It has been shown by explicit calculations within the non-relativistic approach [34] that it is justified to use the diagonal approximation:

$$\Sigma_{kl}^e(\varepsilon) = \delta_{kl}\Sigma_k^e(\varepsilon). \quad (27)$$

Thus, within the diagonal approximation of the self-energy (27) the exact Green's function  $G$  is also diagonal in the Dirac basis and the Dyson equation forms for each  $k$  a non-linear eigenvalue equation

$$(\varepsilon - \varepsilon_k - \Sigma_k^e(\varepsilon))G_k(\varepsilon) = 1. \quad (28)$$

The poles of the Green's function  $G_k(\varepsilon)$  correspond to the zeros of the function

$$f(\varepsilon) = \varepsilon - \varepsilon_k - \Sigma_k^e(\varepsilon). \quad (29)$$

In Refs. [34, 51] it is shown how this problem can be solved by a matrix diagonalization. For each quantum number  $k$  there exist several solutions  $\varepsilon_k^{(\lambda)}$  characterized by the index  $\lambda$ . Because of the coupling to the collective vibrations the single-particle state  $k$  is fragmented as it will be shown in the application in section V A.

#### IV. THE RESPONSE FUNCTION

Nuclear dynamics of an even-even nucleus in a weak external field is described by the linear response function  $R(14, 23)$ , where  $1 = \{k_1, t_1\}$  combines the quantum numbers  $k$  and the time. This response function is the solution of the Bethe-Salpeter equation (BSE) in the  $ph$  channel:

$$R(14, 23) = R^0(14, 23) - i \sum_{5678} R^0(16, 25)V(58, 67)R(74, 83), \quad (30)$$

with the free response  $R^0(14, 23) = G(1, 3)G(4, 2)$ , where function  $G$  is the exact single-particle Green's function. The summation over the number indices  $1, 2, \dots$  implies an integration over the respective time variables. and  $V$  is the effective interaction irreducible in the  $ph$ -channel. This interaction is determined as a variational derivative of the full self-energy  $\Sigma$  with respect to the exact single-particle Green's function:

$$V(14, 23) = i \frac{\delta \Sigma(4, 3)}{\delta G(2, 1)}. \quad (31)$$

Since the self-energy in Eq. (16) has two parts  $\Sigma = \tilde{\Sigma} + \Sigma^e$ , the effective interaction  $V$  in Eq. (30) is a sum of the static RMF interaction  $\tilde{V}$  (26) and time-dependent terms

$$V^e(14, 23) = i \frac{\delta \Sigma^e(4, 3)}{\delta G(2, 1)} \quad (32)$$

After a Fourier transformation in time, this time dependence leads to an energy-dependent interaction  $V^e$ . In the Dirac basis (21) it has the form:

$$V_{kl', lk'}^e(\omega, \varepsilon, \varepsilon') = \sum_{\mu, \sigma} \frac{\sigma \gamma_{k'k}^{\mu(\sigma)*} \gamma_{l'l}^{\mu(\sigma)}}{\varepsilon - \varepsilon' + \sigma(\Omega^\mu - i\eta)}. \quad (33)$$

where  $\sigma = +1$  for empty states and  $-1$  for occupied states (for details see Ref. [52]). The Bethe-Salpeter equation (30) contains the exact Greens' function  $G$ . In order to simplify this equation for the further analysis the  $G$  is expressed it in terms of the mean field Green's function  $\tilde{G}$ . From Eq. (22) we derive the Nambu form for it:

$$\tilde{G}^{-1}(1, 2) = G^{-1}(1, 2) + \Sigma^e(1, 2), \quad (34)$$

which reads in Fourier space as

$$\tilde{G}_{k_1 k_2}(\varepsilon) = \frac{\delta_{k_1 k_2}}{\varepsilon - \varepsilon_{k_1} + i\sigma_{k_1}\eta}. \quad (35)$$

Introducing  $\tilde{R}^0(14, 23) = \tilde{G}(1, 3)\tilde{G}(4, 2)$  one can rewrite Eq. (30) as follows:

$$R = \tilde{R}^0 - i\tilde{R}^0 W R, \quad (36)$$

where  $W$  is a new interaction of the form

$$W = \tilde{V} + W^e \quad (37)$$

with

$$W^e(14, 23) = V^e(14, 23) + i\Sigma^e(1, 3)\tilde{G}^{-1}(4, 2) + i\tilde{G}^{-1}(1, 3)\Sigma^e(4, 2) - i\Sigma^e(1, 3)\Sigma^e(4, 2). \quad (38)$$

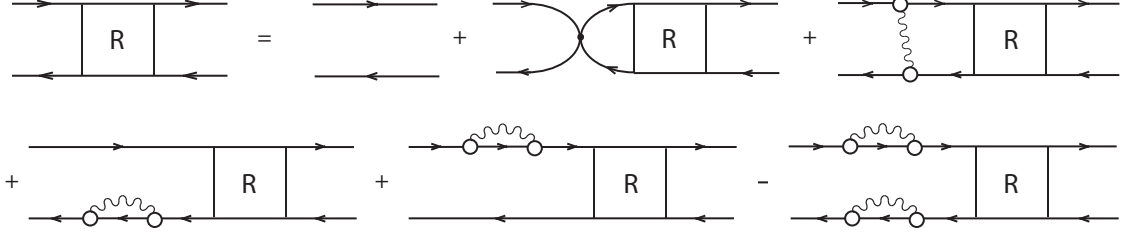


FIG. 2: Bethe-Salpeter equation for the  $ph$ -response function  $R$  in graphical representation. Details are given in Fig. 1 and the small black circle means the static part of the residual  $ph$ -interaction (26).

The graphical representation of the Eq. (36) is shown in Fig. 2.

In addition to the static interaction  $\tilde{V}$  the effective interaction  $W$  contains diagrams with energy-dependent self-energies and an energy-dependent *induced interaction*, where a phonon is exchanged between the particle and the hole. As discussed in Refs. [44–46, 52] the term  $i\Sigma^e(3, 1)\Sigma^e(2, 4)$  has to be neglected in the time blocking approximation if one neglects backward-going propagators caused by the particle-phonon coupling. This is a reasonable approximation applied and discussed in many non-relativistic models (see e.g. Refs. [39–48] and references therein). We have to emphasize, however, that all the RPA ground state correlations are taken into account, because it is well known that they play a central role for the conservation of currents and sum rules.

It turns out that both the solution Eq. (36)  $R$  and its kernel  $W$  are singular. Another difficulty arises because Eq. (36) contains integrations over all time points in the intermediate states. This means that many configurations are contained in the exact response function which are actually more complex than  $1p1h \otimes phonon$ . Tselyaev has introduced in the Ref. [44] the Time Blocking Approximation (TBA), a special time-projection technique to block the  $ph$ -propagation through these complex intermediate states. In this way one obtains after a Fourier transformation in time a relatively simple algebraic equation:

$$R(\omega) = \tilde{R}^0(\omega) + \tilde{R}^0(\omega)\bar{W}(\omega)R(\omega), \quad (39)$$

where

$$\bar{W}_{k_1k_4,k_2k_3}(\omega) = \tilde{V}_{k_1k_4,k_2k_3} + \Phi_{k_1k_4,k_2k_3}(\omega) - \Phi_{k_1k_4,k_2k_3}(0) \quad (40)$$

and

$$\tilde{R}_{k_1k_4,k_2k_3}^0(\omega) = \tilde{R}_{k_1k_2}(\omega)\delta_{k_1k_3}\delta_{k_2k_4}. \quad (41)$$

$\tilde{R}_{k_1 k_2}(\omega)$  is the mean field propagator:

$$\tilde{R}_{ph}(\omega) = -\frac{1}{\varepsilon_{ph} - \omega}, \quad \tilde{R}_{\alpha h}(\omega) = -\frac{1}{\varepsilon_{\alpha h} - \omega}, \quad (42)$$

$$\tilde{R}_{hp}(\omega) = -\frac{1}{\varepsilon_{ph} + \omega}, \quad \tilde{R}_{h\alpha}(\omega) = -\frac{1}{\varepsilon_{\alpha h} + \omega}, \quad (43)$$

$\varepsilon_{ph} = \varepsilon_p - \varepsilon_h$  and  $\Phi$  is the particle-phonon coupling amplitude with the following components:

$$\begin{aligned} \Phi_{ph',hp'}(\omega) = & \sum_{\mu} \left[ \delta_{pp'} \sum_{h''} \frac{\gamma_{h''h}^{\mu} \gamma_{h''h'}^{\mu*}}{\omega - \varepsilon_p + \varepsilon_{h''} - \Omega^{\mu}} \right. \\ & + \delta_{hh'} \left( \sum_{p''} \frac{\gamma_{pp''}^{\mu} \gamma_{p'p''}^{\mu*}}{\omega - \varepsilon_{p''} + \varepsilon_h - \Omega^{\mu}} + \sum_{\alpha''} \frac{\gamma_{p\alpha''}^{\mu} \gamma_{p'\alpha''}^{\mu*}}{\omega - \varepsilon_{\alpha''} + \varepsilon_h - \Omega^{\mu}} \right) \\ & \left. - \left( \frac{\gamma_{pp'}^{\mu} \gamma_{hh'}^{\mu*}}{\omega - \varepsilon_{p'} + \varepsilon_h - \Omega^{\mu}} + \frac{\gamma_{p'p}^{\mu*} \gamma_{h'h}^{\mu}}{\omega - \varepsilon_p + \varepsilon_{h'} - \Omega^{\mu}} \right) \right], \end{aligned} \quad (44)$$

$$\begin{aligned} \Phi_{\alpha h',h\alpha'}(\omega) = & \sum_{\mu} \left[ \delta_{\alpha\alpha'} \sum_{h''} \frac{\gamma_{h''h}^{\mu} \gamma_{h''h'}^{\mu*}}{\omega - \varepsilon_{\alpha} + \varepsilon_{h''} - \Omega^{\mu}} \right. \\ & + \delta_{hh'} \left( \sum_{\alpha''} \frac{\gamma_{\alpha\alpha''}^{\mu} \gamma_{\alpha'\alpha''}^{\mu*}}{\omega - \varepsilon_{\alpha''} + \varepsilon_h - \Omega^{\mu}} + \sum_{p''} \frac{\gamma_{\alpha p''}^{\mu} \gamma_{\alpha' p''}^{\mu*}}{\omega - \varepsilon_{p''} + \varepsilon_h - \Omega^{\mu}} \right) \\ & \left. - \left( \frac{\gamma_{\alpha\alpha'}^{\mu} \gamma_{hh'}^{\mu*}}{\omega - \varepsilon_{\alpha'} + \varepsilon_h - \Omega^{\mu}} + \frac{\gamma_{\alpha'\alpha}^{\mu*} \gamma_{h'h}^{\mu}}{\omega - \varepsilon_{\alpha} + \varepsilon_{h'} - \Omega^{\mu}} \right) \right]. \end{aligned} \quad (45)$$

As in Fig. 1 the indices  $p, \alpha$  and  $h$  denote the particles, antiparticles and holes in the Dirac basis. The amplitudes  $\Phi_{ph',h\alpha}$ ,  $\Phi_{\alpha h',hp}$  are neglected, because they have only a small effect (see Ref. [51]). The amplitudes  $\Phi_{pp',hh'}$  and  $\Phi_{hh',pp'}$  are also disregarded within this approximation. Therefore, ground state correlations are taken into account only on the RPA level due to the presence of the  $\tilde{V}_{pp',hh'}$ ,  $\tilde{V}_{hh',pp'}$  terms of the static interaction in the Eq. (39). By definition, the response function  $R(\omega)$  in Eq. (39) contains only configurations which are not more complex than  $1p1h \otimes \text{phonon}$ .

In Eq. (39)  $\Phi(0)$  is subtracted from  $\Phi(\omega)$ . This corresponds to the subtraction procedure developed by Tselyaev in Ref. [47]. It considers the fact that the effective interaction  $\tilde{V}$  being adjusted to experimental data of the ground state contains effectively many correlations and, in particular, also admixtures of phonons at the energy  $\omega = 0$ . In the present method, all correlations entering through the admixture of phonons are taken care of by the additional interaction term  $\Phi(\omega)$ . To avoid double counting in the effective interaction the part  $\Phi(0)$  is therefore subtracted. This means only the energy dependence of the phonon coupling is effectively taken into account.

To describe the observed spectrum of the excited nucleus in a weak external field  $D$ , as for instance a dipole field, one needs to calculate the strength function:

$$S(E) = -\frac{1}{\pi} \lim_{\Delta \rightarrow +0} \text{Im} \Pi_{DD}(E + i\Delta), \quad (46)$$

expressed through the polarizability

$$\Pi_{DD}(\omega) = D^\dagger R(\omega) D \quad (47)$$

A finite imaginary part  $\Delta$  of the energy variable is introduced in the calculations for convenience in order to obtain a more smoothed envelope of the spectrum. This parameter has the meaning of an additional artificial width for each excitation. This width emulates effectively contributions from configurations which are not taken into account explicitly in this approach.

In order to calculate the strength function it is convenient to convolute Eq. (39) with an external field operator and introduce the transition density matrix  $\delta\rho$  in the external field  $D$ :

$$\delta\rho_{k_1 k_2}(\omega) = \sum_{k_3 k_4} R_{k_1 k_4, k_2 k_3}(\omega) D_{k_3 k_4}, \quad (48)$$

$$\delta\rho_{k_1 k_2}^0(\omega) = \sum_{k_3 k_4} \tilde{R}_{k_1 k_4, k_2 k_3}^0(\omega) D_{k_3 k_4}, \quad (49)$$

Using Eq. (39) we find that  $\delta\rho(\omega)$  obeys the equation

$$\delta\rho(\omega) = \delta\rho^0(\omega) + \tilde{R}^0(\omega) \left( \tilde{V} + \Phi(\omega) - \Phi(0) \right) \delta\rho(\omega), \quad (50)$$

and the strength function is expressed as

$$S(E) = -\frac{1}{\pi} \lim_{\Delta \rightarrow +0} \text{Im} \text{Tr}[D^\dagger \delta\rho(E + i\Delta)]. \quad (51)$$

## V. APPLICATIONS

For the following applications discussed in this section the parameter set NL3 [71] is used for the covariant energy functional. For superfluid nuclei we use in the pairing channel a simple monopole force with the strength parameters  $G_\tau$  ( $\tau = p, n$ ) adjusted to experimental gap parameters for protons and neutrons. The cut-off energy in the pairing channel is 20 MeV both for protons as well as for neutrons. The parameter set NL3 has been adjusted to ground state properties of a few spherical nuclei more than ten years ago. In numerous applications it has been shown that it provides on the mean field level a very good description of ground states and excited states of nuclei all over the periodic table [72]. In a recent investigation [73] its parameters have been slightly modified and several small deficiencies have been eliminated.

### A. Single-particle spectra in the Pb-region

In this section we discuss the changes of the single-particle spectra of the odd mass nuclei  $^{207}\text{Pb}$ ,  $^{209}\text{Pb}$ ,  $^{207}\text{Tl}$  and  $^{209}\text{Bi}$  if the coupling to low lying collective vibrations of the surface is taken into



TABLE I: Energies  $\varepsilon_k^{(d)}$  and spectroscopic factors  $S_k^{(d)}$  of the dominant neutron levels in  $^{208}\text{Pb}$  calculated in the strongly restricted particle-phonon space.  $ph\alpha$  denotes full the calculation,  $p\alpha$  ( $h$ ) is the version without backwards going terms, and  $ph$  is the version without contribution of the antiparticle states in the self-energy (see text for details).

State $k$	$\varepsilon_k$ , MeV	$\varepsilon_k^{(d)}$ , MeV			$S_k^{(d)}$		
Particle		$ph\alpha$	$p\alpha$	$ph$	$ph\alpha$	$p\alpha$	$ph$
2g9/2	-2.50	-2.85	-3.14	-2.88	0.89	0.92	0.89
1i11/2	-2.97	-2.82	-3.20	-2.90	0.94	0.97	0.94
1j15/2	-0.48	-1.16	-1.33	-1.21	0.70	0.74	0.70
3d5/2	-0.63	-0.96	-1.05	-0.98	0.93	0.94	0.93
4s1/2	-0.36	-0.88	-0.92	-0.89	0.93	0.93	0.93
2g7/2	-0.56	-0.71	-0.90	-0.76	0.92	0.94	0.92
3d3/2	-0.02	-0.35	-0.42	-0.37	0.93	0.93	0.93
Hole		$ph\alpha$	$h$	$ph$	$ph\alpha$	$h$	$ph$
3p1/2	-7.66	-7.67	-7.40	-7.70	0.96	0.98	0.96
2f5/2	-9.09	-8.97	-8.71	-9.02	0.93	0.96	0.93
3p3/2	-8.40	-8.20	-7.87	-8.22	0.90	0.94	0.90
1i13/2	-9.59	-9.30	-9.07	-9.36	0.90	0.92	0.89
2f7/2	-11.11	-10.20	-9.98	-10.22	0.72	0.76	0.72
(1h9/2) <sub>1</sub>	-13.38	-13.32	-13.23	-13.34	0.52	0.47	0.53
(1h9/2) <sub>2</sub>		-12.48	-12.42	-12.49	0.31	0.39	0.29

account. In order to keep the numerical effort in reasonable limits in a first investigation only the most collective phonons with spin and parity  $J^\pi = 2^+, 3^-, 4^+, 5^-, 6^+$  below the neutron separation energy and a reduced number of single-particle states with positive energy (particles or holes) is taken into account in the solution of the Dyson equation (28). This reduces strongly the number of poles in the self-energy of Eq. (23). The numerical results obtained in these investigations are compiled in the Table I. For the first shell of neutron levels above ('particle') and below ('hole') the Fermi level three versions are given: in the version  $ph\alpha$  the index  $n$  in Eq. (23) includes all contributions from intermediate states above the Fermi level  $p$ , below the Fermi level  $h$  and in the Dirac sea  $\alpha$ . Version  $p\alpha$  (for particles) or  $h$  (for holes) excludes the backward going diagrams, and

the third version *ph* does not contain antiparticle intermediate states in (23). In this way, one can see that the effects of ground state correlations (GSC) caused by the particle-phonon coupling and neglected in the second version are significant and it is essential to take them into account in a realistic calculation. On the other hand, the contribution of the antiparticle subspace to the self-energy is quantitatively not of great importance. This can be understood by the large values of the energy denominators in Eq. (23) for these configurations. Thus it is justified to disregard them in the following calculations. Notice, however, that version *ph* does not eliminate the effects of the Dirac sea completely since the phonon vertices still contain this contribution. As it has been discussed in Ref. [24] these terms play an important role in a proper treatment of relativistic RPA. Otherwise it is not possible to obtain reasonable properties for the isoscalar modes within RRPA.

Next we show results where the contribution of the antiparticle subspace to the self-energy are neglected. In this case one is able to enlarge the particle-hole basis considerably by taking into account particle-hole configurations far away from the Fermi surface. This increases the collectivity of the phonons and, consequently, the strength of the particle-vibrational coupling. The phonon basis was also enriched by including higher-lying modes up to 35 MeV. Solving the Dyson equation one finds a fragmentation of the single-particle states and a corresponding reduction of the single-particle strength. For the levels one major shell below and one shell above the Fermi surface one finds always one dominant level, which is shifted against the corresponding single-particle energy without particle-phonon coupling. Almost all the levels are moving downwards providing thus a considerably better agreement with experimental energies than the pure RMF states. In the next shells further away from the Fermi surface almost all the single-particle levels turn out to be strongly fragmented due to phonon coupling and it is no longer possible to determine the dominant levels in these shells, in other words, the concept of Landau quasi-particles is defined only in the neighborhood of the Fermi level and it breaks down at larger distances.

In Fig. 3 we show as an example the  $3d_{3/2}$  and the  $1j_{15/2}$  levels in the nucleus  $^{209}\text{Pb}$ . In both cases the single-particle strength is distributed over about two thousand states but most of them are vanishingly small. Thus only the states with the strength exceeding  $10^{-3}$  are drawn. The state  $3d_{3/2}$  has a pronounced single-particle structure with a single-particle strength close to 0.9. On the other side the  $1j_{15/2}$  is more fragmented. The experimental strength of the dominant levels are shown with dashed lines.

To illustrate the shifts in the level schemes of the dominant poles as compared to the RMF results we show as an example in Figs. 4 the single-particle spectrum for neutrons. The spectrum calculated with the energy-dependent correction (RMF+PVC) demonstrates a pronounced increase

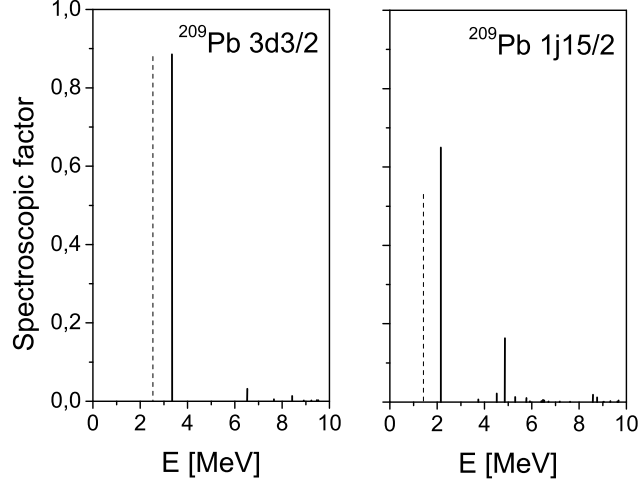


FIG. 3: Single-particle strength distribution for the  $3d_{3/2}$  (left panel) and  $1j_{15/2}$  (right panel) states in  $^{209}\text{Pb}$  obtained in the calculations (solid lines) and the experimental strengths of the respective dominant levels (dashed lines).

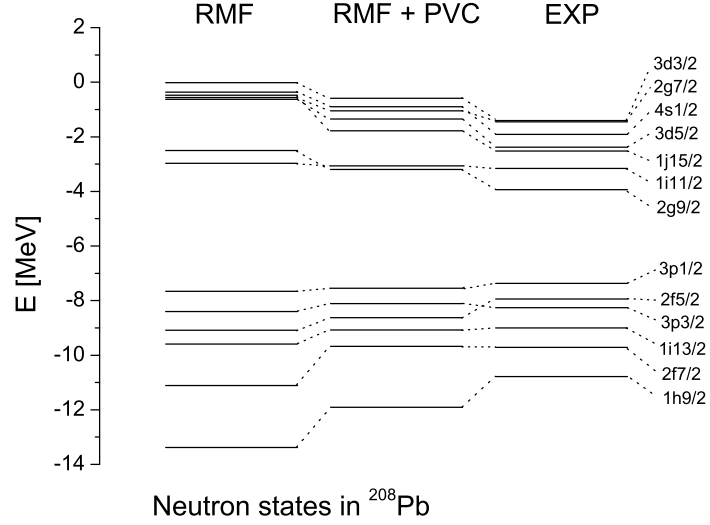


FIG. 4: Neutron single-particle states in  $\text{Pb}^{208}$ : the pure RMF spectrum (left column), the levels computed within RMF with allowance for the particle-vibration coupling (center) and the experimental spectrum (right).

of the level density around the Fermi surface of  $^{208}\text{Pb}$  compared the pure RMF spectra. In some cases the order of levels is inverted and the observed sequence is reproduced as for instance for the  $1j_{15/2}$  and the  $3d_{5/2}$  neutron states. Another and more important example is the inversion of the  $2g_{9/2}$  and  $1i_{11/2}$  neutron states which reproduces the spin of the  $^{209}\text{Pb}$  ground state.

In order to quantify these results we calculate the average distance between two levels in the spectrum shown in Fig. 4. One finds for the neutrons 1.0 (RMF), 0.83 (RMF+PCV) and 0.76 (EXP) in units of MeV. This corresponds to a level density of 1.0 (RMF), 1.20 (RMF+PCV) and 1.31 (EXP) in units of  $\text{MeV}^{-1}$ . The level density in the neighborhood of the Fermi surface is therefore in RMF-calculations by a factor 0.76 smaller than the experimental value. Taking into account particle-vibrational coupling we find only a reduction of 0.92. Assuming an effective mass close to 1 for the experiment, and taking into account that the level density at the Fermi surface is proportional to  $m^*/m$ , this corresponds to an effective mass  $m^*/m \approx 0.76$  for the RMF and  $m^*/m \approx 0.92$  for the RMF+PCV calculations. For the protons the situation is similar.

Jaminon and Mahaux have discussed in Refs. [74, 75] the concept of the effective mass in the case of RMF theory. On one side one has the well known Dirac mass

$$m_D = m + \tilde{\Sigma}_s(\mathbf{r}), \quad (52)$$

which is determined by the scalar field  $\tilde{\Sigma}_s$ . Since we do not use an isovector scalar field for the present parameter set NL3 the Dirac mass is in these calculations identical for protons and neutrons. However, this quantity should not be compared with the effective mass determined empirically from a non-relativistic analysis of scattering data and of bound states. From a non-relativistic approximation of the Dirac equations one finds that the mass

$$m_{eff} = m - \tilde{\Sigma}_0 \quad (53)$$

should be used for this purpose. Here  $\tilde{\Sigma}_0$  is the time-like component of the Lorentz vector field determined by the exchange of  $\omega$ - and  $\rho$ -mesons.

In symmetric nuclear matter we find for NL3:  $m_D/m = 0.60$  and  $m_{eff}/m = 0.67$ . The latter value is smaller than the values  $m^*/m \approx 0.71$  for protons and  $m^*/m \approx 0.76$  for neutrons deduced from the calculated spectrum around the Fermi surface in simple RMF theory. Following similar arguments we would obtain for RMF+PVC calculations an average effective mass of 0.89. This is obviously still too low as compared to the experimental value.

On the other hand, around the Fermi surface where relativistic kinematic effects are not significant the RMF+PVC spectrum can be characterized by the effective mass deduced from the Schrödinger equation which is a non-relativistic limit of the Dirac equation (15). In this approximation one can calculate the state-dependent E-mass  $\bar{m}/m^{RMF}$  which is the inverted spectroscopic factor of the dominant level  $\lambda$ :

$$\frac{\bar{m}_k}{m^{RMF}} = [S_k^{(\lambda)}]^{-1}. \quad (54)$$

For the calculated RMF+PVC spectrum the averaged E-masses are 1.26 for neutrons and 1.41 for protons if one takes into account all the states with spectroscopic factors larger than 0.5, i. e. good single-particle states. Thus, the energy dependence of the self-energy increases the RMF neutron and proton effective masses up to the values 0.96 and 1.0, respectively.

Although the problem of particle-vibration coupling in nuclei has a long history and it was considered in a number of works, most of them are based on a non-relativistic treatment of the nuclear many-body problem. Only in a relatively recent investigation in Ref. [76] a correction of the RMF single-particle spectrum was undertaken in a phenomenological way assuming a linear dependence of the self-energy near the Fermi surface. The corresponding coupling constants were determined by a fit to nuclear ground state properties. Despite the fact that the present approach is fully microscopic without any additional parameter adjusted to experiment it shows good agreement with the results of Ref. [76] for the spectrum of  $^{208}\text{Pb}$ . The shift caused by the phenomenological particle-vibrational coupling in Ref. [76] is only slightly larger than in the present investigation.

Non-relativistic microscopic investigations of particle-vibrational coupling can be divided into two major groups. The first group [34, 35, 70, 77] uses a phenomenological single-particle input to reproduce the experimental spectrum and has therefore to exclude the contribution of the particle-vibration coupling from the full self-energy to find the 'bare' spectrum. Usually these older approaches take into consideration only a relatively small number of collective low-lying phonons and use a particle-vibration coupling model [36]. This restriction to only low-lying modes produces shifts less than 1 MeV. However, as it was shown in Ref. [35], enlarging of the phonon space with high-lying vibrations leads to very strong shifts of the single-particle levels up to 4 MeV, and no saturation is observed with respect to the dimension of the phonon space.

The second group of approaches (see, for instance Refs. [78, 79]) starts from a self-consistent Hartree-Fock description and applies perturbation theory to calculate the particle-vibration contribution to the full self-energy. In such self-consistent methods it is more justified to enlarge the phonon space. It was shown, for instance, in [79] that the contribution of the isovector modes is noticeably smaller than the isoscalar ones. The detailed investigation of the relative importance of the high multipole states was performed in [78]. Because of the larger phonon space the typical shifts of the single-particle levels in  $^{208}\text{Pb}$  are about 1-2 MeV.

As for the spectroscopic factors, all the approaches predict similar values because these factors are not very sensitive to the details of the calculation schemes.

### B. The strength functions of collective excitations in closed shell nuclei

The solution of the Bethe-Salpeter equation (39) allows to calculate the nuclear response to external multipole fields and the strength functions of the corresponding collective excitations. As in the last section we show applications based on the density functional NL3 with a monopole force in the pairing channel. A small artificial width of 200 keV is introduced as an imaginary part of the energy variable  $\omega$  to have a smooth envelope of the calculated curves. The energies and amplitudes of the most collective phonon modes with spin and parity  $2^+$ ,  $3^-$ ,  $4^+$ ,  $5^-$ ,  $6^+$  are calculated with the same restrictions and selected using the same criterion as in the last section and in many other non-relativistic investigations in this context. Only the phonons with energies below the neutron separation energy enter the phonon space since the contributions of the higher-lying modes are found to be small.

On all three stages of these calculations the same energy functional, i.e. the same relativistic nucleon-nucleon interaction  $\tilde{V}$  (26) has been employed. The vertices  $\gamma_{k_1 k_2}^\mu$  (25) entering the term  $\Phi(\omega)$  in Eq. (44) are calculated with the same force. Therefore no further parameters are needed. The scheme is fully consistent.

The subtraction procedure developed by Tselyaev in the Ref. [47] for the self-consistent scheme removes the static contribution of the particle-phonon coupling from the  $ph$ -interaction. It takes into account only the additional energy dependence introduced by the dynamics of the system. It has been found in the calculations of Refs. [48] as well as in the calculations of the Ref. [11] that within the relatively large energy interval (0 - 30 MeV) the subtraction procedure provides a rather small increase of the mean energy of the giant dipole resonance (0.8 MeV for lead region) and gives rise to the change by a few percents in the sum rule. This procedure restores the response at zero energy and therefore it does not disturb the symmetry properties of the RRPA calculations. The zero energy modes connected with the spontaneous symmetry breaking in the mean field solutions, as for instance the translational mode in the dipole case, remain at exactly the same position after the inclusion of the particle-vibration coupling. In practice, however, because of the limited number of oscillator shells in the calculations this state is found already in RRPA without particle-vibration coupling at a few hundreds keV above zero. In cases, where the results depend strongly on a proper separation of this spurious state, as for instance for investigations of the pygmy dipole resonance in neutron rich systems [53, 80] one has to include a large number of  $ph$ -configurations in the RRPA solution.

In Fig. 5 we show the calculated strength functions for the isoscalar monopole resonance in

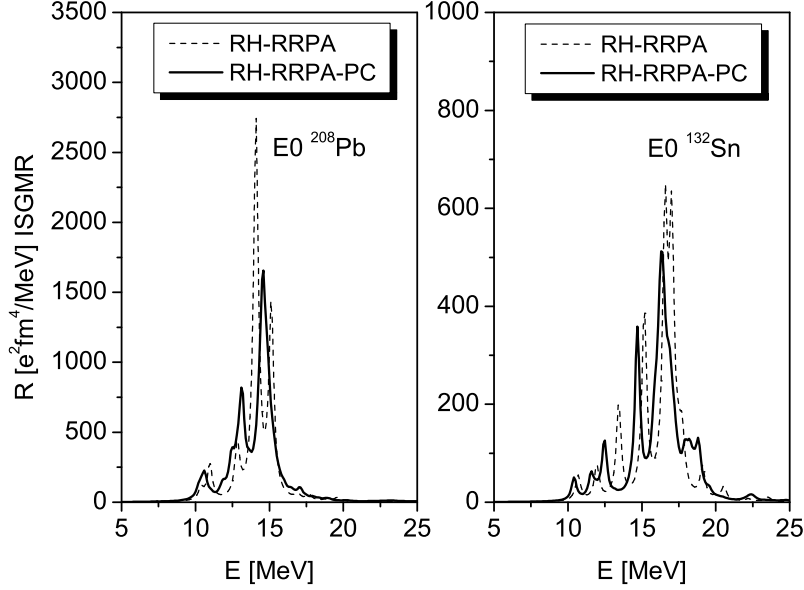


FIG. 5: Isoscalar monopole resonance in  $^{208}\text{Pb}$  and  $^{132}\text{Sn}$  obtained within two approaches: RRPA (dashed line) and RRPA with particle-phonon coupling RRPA-PC (solid line). Both computations have been performed with relativistic Hartree (RH) mean field and employ NL3 parameter set for RMF forces.

TABLE II: Lorentz fit parameters of isoscalar E0 strength function in  $^{208}\text{Pb}$  and  $^{132}\text{Sn}$  calculated within RRPA and RRPA extended by the particle-phonon coupling model (RRPA-PC) as compared to experimental data. The fit has been carried out in the interval from  $B_n$  to roughly 20 MeV

		$\langle E \rangle$ (MeV)	$\Gamma$ (MeV)
$^{208}\text{Pb}$	RRPA	14.16	1.71
	RRPA-PC	14.05	2.36
	Exp. [81]	13.73(20)	2.58(20)
$^{132}\text{Sn}$	RRPA	16.10	2.63
	RRPA-PC	16.01	3.09

$^{208}\text{Pb}$  and  $^{132}\text{Sn}$ . The fragmentation of the resonance caused by the particle-phonon coupling is clearly demonstrated although the spreading width of the monopole resonance is not large because of a strong cancellation between the self-energy diagrams and diagrams with the phonon exchange (see Fig. 2). This fact has also been discussed in detail in Refs. [39, 40] and it is not disturbed by

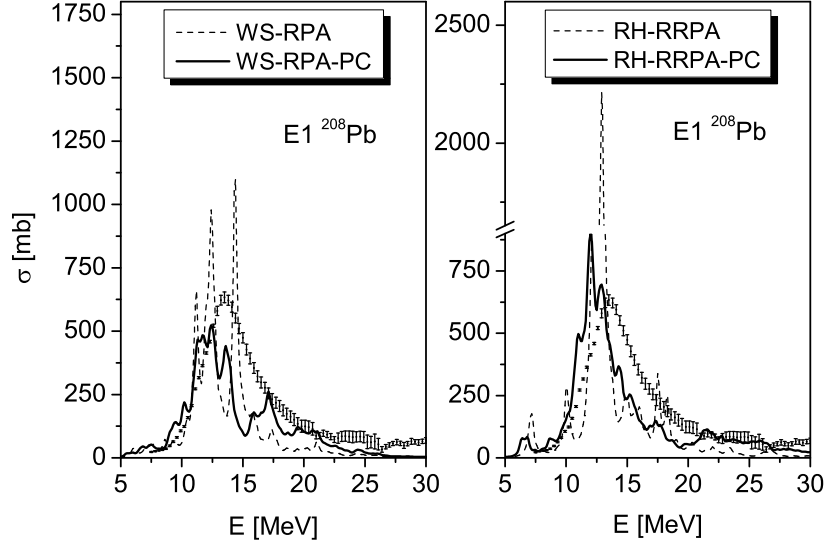


FIG. 6: The isovector E1 resonance in  $^{208}\text{Pb}$ . Details are given in the text.

the subtraction procedure because this cancellation takes place as well in  $\Phi(\omega)$  as in  $\Phi(0)$ .

In order to compare the spreading of the theoretical strength distributions with experimental data we show in Table II mean energies  $\langle E \rangle$  and widths parameters  $\Gamma$  obtained by fitting the theoretical strength distribution in a certain energy interval to a Lorentz curve in the same way as it has been done in the experimental investigations. The experimental values shown in Table II are derived in the Ref. [81] from the evaluation of a series of data obtained in different experiments for the isoscalar monopole resonance in  $^{208}\text{Pb}$ .

Figs. 6 and 7 present calculated photoabsorption cross sections

$$\sigma_{E1}(E) = \frac{16\pi^3 e^2}{9\hbar c} E S_{E1}(E) \quad (55)$$

for the isovector dipole resonance in  $^{208}\text{Pb}$  and in  $^{132}\text{Sn}$ . The left panels give the results obtained within the non-relativistic approach with a Woods-Saxon (WS) single-particle potential and Landau-Migdal (LM) forces described in Ref. [48]. They are compared in the right panel with the relativistic fully consistent theory of Ref. [52]. (R)RPA calculations are shown by the dashed curves, (R)RPA extended by the phonon coupling ((R)RPA-PC) calculations – by the thick solid curves. In Fig. 6 we have also displayed experimental data with error bars taken from Ref. [82]. In both calculations, relativistic (right panel) and non-relativistic (left panel), the continuum is taken into account only in a discrete approximation, which is very reliable for heavy nuclei. As discussed in Ref. [14], the Dirac equation (21) is solved in an oscillator basis. To make the comparison reasonable calculations within the non-relativistic framework have been performed with



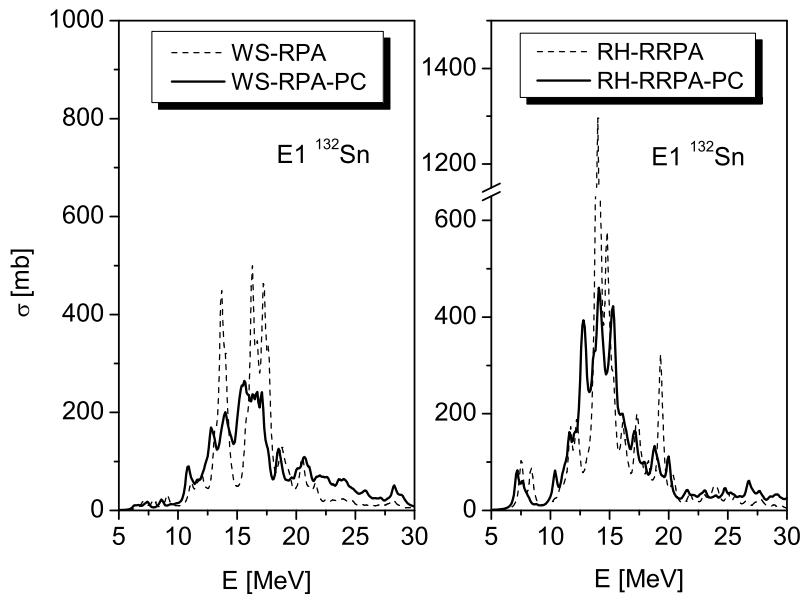


FIG. 7: The same as in Fig. 6 but for  $^{132}\text{Sn}$ .

box boundary conditions for the Schrödinger equation in  $r$ -space which ensures completeness of the single-particle basis.

The corresponding Lorentz fit parameters in the two energy intervals:  $B_n - 25$  MeV and  $0 - 30$  MeV ( $B_n$  is the neutron separation energy) are included in Table III and they are compared with the data of Ref. [82, 83]. We notice that the inclusion of particle-phonon coupling in the RRPA calculation induces a pronounced fragmentation of the photoabsorption cross sections, and brings the width of the GDR in much better agreement with the data, both for  $^{208}\text{Pb}$  and  $^{132}\text{Sn}$ .

The fragmentation of the resonance introduced by the particle-phonon coupling is clearly demonstrated in both cases. Also, one finds more or less the same level of agreement between theory and experimental data for these two calculations. In the case of the isovector E1 resonance in  $^{132}\text{Sn}$  this is, however, not so clear because the cross section and the integral characteristics of the resonance obtained in the experiment of Ref. [83] are given with relatively large error bars. In  $^{208}\text{Pb}$  the self-consistent relativistic approach reproduces the shape of the giant dipole resonance much better than the non-relativistic one although the whole resonance is about 0.5 MeV shifted to lower energies with respect to the experiment. As one can see from the Fig. 6 and Table III, we observe some shift already in the RRPA calculation, which is determined by the properties of the NL3 forces. Improvement of the forces, for instance, the use of the density dependent versions [84, 85] of the RMF should bring the E1 mean energy in better agreement with the data.

TABLE III: Lorentz fit parameters in the two energy intervals:  $B_n - 25$  MeV and  $0 - 30$  MeV, for the E1 photo absorption cross sections in  $^{208}\text{Pb}$  and  $^{132}\text{Sn}$ , calculated with the RRPA, and with the RRPA extended to include the particle-phonon coupling (RRPA-PC), compared to data.

		$B_n - 25$ MeV			$0 - 30$ MeV		
		$\langle E \rangle$	$\Gamma$	EWSR	$\langle E \rangle$	$\Gamma$	EWSR
		(MeV)	(MeV)	(%)	(MeV)	(MeV)	(%)
$^{208}\text{Pb}$	RRPA	13.1	2.4	121	12.9	2.0	128
	RRPA-PC	12.9	4.3	119	13.2	3.0	128
	Exp. [82]	13.4	4.1	117			125(8)
$^{132}\text{Sn}$	RRPA	14.7	3.3	116	14.5	2.6	126
	RRPA-PC	14.4	4.0	112	14.6	3.2	126
	Exp. [83]	16.1(7)	4.7(2.1)	125(32)			

However, there is an essential difference between the fully self-consistent relativistic calculations and the non-relativistic approach: in non-relativistic approach discussed in Ref. [48] one introduces on all three stages of the calculation phenomenological parameters, which have to be adjusted to experimental data: first, the Woods-Saxon parameters as, for instance, the well depth are varied to obtain single-particle levels close to the experimental values, second, one of the parameters of the Landau-Migdal force is adjusted to get phonon energies at the experimental positions (for each mode) and, third, another Landau-Migdal force parameter is varied to reproduce the centroid of the giant resonance. Although the varying of the parameters is performed in relatively narrow limits, it is necessary to obtain realistic results. In contrast, in the relativistic fully consistent approach no adjustment of additional parameters is necessary. Of course, the underlying energy functional has been determined in a phenomenological way by a fit to experimental ground state properties of characteristic nuclei. However, it is of universal nature and the same parameters are used for investigations of many nuclear properties all over the periodic table. The predictive power of this scheme is therefore much higher than that of the present semi-phenomenological approach discussed, for instance, in Ref. [48].

### C. Collective excitations in systems with pairing

Pairing correlations play an essential role in all open shell nuclei and apart from the vicinity of the very few doubly magic configurations nuclei show superfluidity all over the periodic table. In a theoretical description this fact can be taken into account by Bogoliubov's quasiparticles. Many-body theories for normal systems are thus relatively easily extended to the case of superfluid nuclei. Combining creation and annihilation operators  $a^+$  and  $a$  to a two-component operator, operators of the type  $a^+a$ ,  $a^+a^+$ ,  $aa$  are replaced by super-matrices of rank 2 and the form of the equations stays nearly unchanged. This very elegant method has been introduced already half a century ago in Ref. [86] and over the years it has been used for various many-body approximation schemes in non-relativistic systems as for instance in Refs. [10, 87–89]. Response theory with the Time Blocking Approximation (TBA) introduced for normal non-relativistic systems in Ref. [44] has been extended in Refs. [47, 48] to QTBA for superfluid systems and in Ref. [11] to RQTBA for relativistic superfluid systems.

In the following we discuss several applications of RQRPA and of RQTBA in the chain of spherical even-even semi-magic nuclei with  $Z = 50$ . We show calculations of the isovector dipole spectrum in the giant dipole resonance region and in the low-lying energy region in the two approximations.

As discussed before the effective interaction  $\Phi(\omega)-\Phi(0)$  takes into account only the additional energy dependence introduced by the dynamics of the system. It has been found in relativistic [11] as well as in non-relativistic calculations [48] that within a relatively large energy interval (0 - 30 MeV) the subtraction procedure provides a rather small but noticeable increase of the mean energy of the giant dipole resonance (about 0.7 MeV for tin region) and gives rise to changes by a few percents in the sum rule. The absolute value of the energy shift produced by the subtraction of  $\Phi(0)$  in Eq. (40) is comparable with but not exactly equal to the absolute value of the shift produced by the dynamical part of the interaction amplitude  $\Phi(\omega)$  which always reduces the mean energy of the resonance. The subtraction procedure restores the response at zero energy and, therefore, it does not disturb the symmetry properties of the RQRPA calculations. The zero energy modes connected with the spontaneous symmetry breaking in the mean field solutions, as, for instance, the translational mode in the dipole case, remain at exactly the same positions after the inclusion of the quasiparticle-vibration coupling.

In Fig. 8 we show dipole spectra for the tin isotopes  $^{116}\text{Sn}$ ,  $^{120}\text{Sn}$ ,  $^{130}\text{Sn}$ . The right panels show the photo absorption cross section (55) which is determined by the dipole strength function  $S_{E1}$ . It is calculated, analogously to Eq. (51), with the usual isovector dipole operator. The left

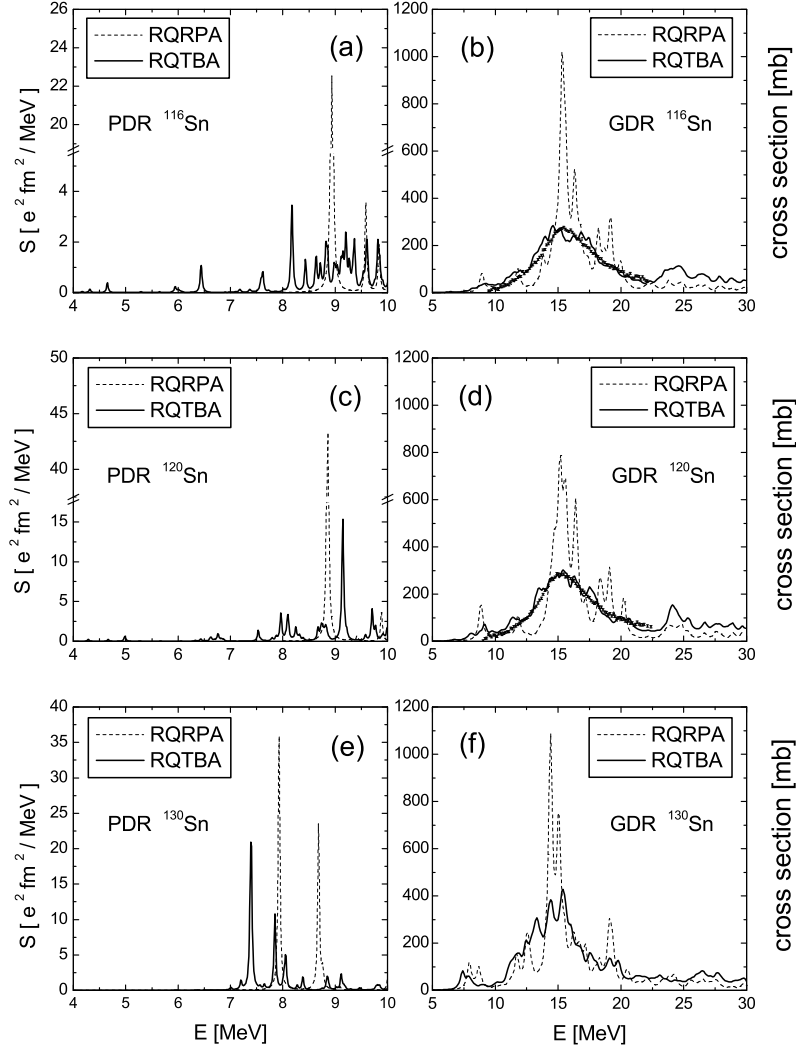


FIG. 8: The calculated dipole spectra for the heavier tin isotopes  $^{116}\text{Sn}$ ,  $^{120}\text{Sn}$ ,  $^{130}\text{Sn}$ , compared to data of Ref. [90] for  $^{116,120}\text{Sn}$ . Right panels (b, d, f): photo absorption cross sections computed with the artificial width 200 keV. Left panels (a, c, e): the low-lying portions of the corresponding spectra in terms of the strength function, calculated with 20 keV smearing. Calculations within the RQRPA are shown by the dashed curves, and the RQTBA - by the solid curves.

panels show the low-lying parts of the corresponding spectrum in terms of the strength function. A small imaginary part of 20 keV is used for the energy variable, in order to see the fine structure of the spectrum and sometimes individual levels in this region. RQRPA calculations are shown by dashed curves and the RQTBA by the solid curves. Experimental data are taken from the EXFOR database [90].

These figures clearly demonstrate how the two-quasiparticle states, which are responsible for

the spectrum of the RQRPA excitations, are fragmented through the coupling to the collective vibrational states. The effect of the particle-vibration coupling on the low-lying dipole strength below and around the neutron threshold within the presented approach is shown in the left panels of the Fig. 8. Such calculations give us an example how the low-lying strength develops with the increase of the neutron excess. It is also found that the presence of pairing correlations causes a noticeably stronger fragmentation of both the GDR and the PDR modes as compared to the case of a normal system discussed above. This effect has the two reasons. First, pairing correlations lead to a diffuseness of the Fermi surface and, thus, increase the number of possible  $2qp \otimes \text{phonon}$  configurations, and second, pairing correlations cause a considerable lowering of the energies and increased transition probabilities of the lowest  $2^+$  states. In spherical open-shell medium mass nuclei the highly collective first  $2^+$  states appear at energies around 1 MeV (and they are usually well reproduced in RQRPA [91]) whereas in magic nuclei and often in nuclei near the shell closures they appear much higher, at about 3-4 MeV and have considerably reduced transition probabilities. This causes a strong configuration mixing in the case of presence of very low-lying vibrational states. These modes admix to others, in particular, to the GDR and the PDR and the lower their energies and the higher their transition probabilities are, the stronger fragmentation they cause.

A systematic analysis of the transition densities of the RQRPA and the RQTBA states shows that the  $2qp$  transition densities in the broad low-lying energy region dominated by the fragmentation of the RQRPA pygmy mode have a very similar behavior as the initial RQRPA state: proton and neutron components oscillate in phase in the nuclear interior and neutron components dominate on the surface in nuclei with noticeable neutron excess.

## VI. CONCLUSIONS

We have given an overview over recent efforts to combine two theoretical methods for the description of the quantum-mechanical many-body problem of nuclear physics, Covariant Density Functional Theory (CDFT) and Landau-Migdal Theory of Finite Fermi Systems (TFFS). Both methods are very successful and they are claimed to provide in principle an exact description. In practice, however, there are limitations. Both methods use phenomenological input. DFT can only be applied to physical quantities, which can be expressed in terms of the single-particle density and in self-bound systems such as nuclei DFT is based on the intrinsic density, a concept, which requires additional approximations. In particular the self-energy used in DFT theory does not depend on the energy. Landau-Migdal theory on the other side restrains itself from calculating ground state

properties, but it goes far beyond the mean field approach and takes into account couplings to complex configurations. There are also similarities for these two methods. Both are based on a single-particle description, i.e. on the motion of independent particles. In density functional theory an average field is introduced as a vehicle in order to take into account shell effects. However, the single-particle energies themselves are not observables in the strict sense. Landau-Migdal theory uses quasiparticles as the exact eigenstates of the  $A \pm 1$ -systems. In both cases the self energies are given as the first derivatives of the total energy with respect to the density and the effective interactions between the particles are the second derivatives of this quantity.

The combination of CDFT and TFFS described in this manuscript starts from the covariant density functional. No further parameters are needed. This functional is used to describe the ground state properties and the parameters of the functional are adjusted to experimental data of ground states of several nuclei. On this level the self-energy does not depend on the energy and Landau-Migdal theory is used to introduce an energy dependence with a particle-vibrational scheme. The properties of the phonons needed for the calculation of the energy-dependent part of the self-energy are phonon energies and phonon-nucleon vertices. They are calculated with the static effective interaction obtained as the second derivative of the density functional. No additional parameters are needed. The essential equation of the Landau-Migdal theory is the response equation. The effective interaction to calculate the full response is the derivative of the self-energy with respect to the density and this means that one obtains in addition to the static interaction resulting from the energy-independent part an induced interaction resulting from the energy-dependent part of the self-energy. Of course there would be double counting, because many of the correlations induced by the coupling of virtual phonons have also contributions at the ground state energy. Therefore a subtraction method is introduced, which removes from the induced interaction at finite energy its value at zero energy, i.e. after this subtraction, the induced interaction vanishes at the ground state and takes into account only its energy dependence. Therefore this subtraction procedure guarantees that one does not need to readjust the parameters of the density functional, because the effects of particle-vibrational coupling vanish at the ground state of the even-even system, where the parameters are adjusted.

We have discussed several applications of this method, as the fragmentation of single-particle energies in odd-mass nuclei in the vicinity of a double magic configuration. Close to the Fermi surface there is always a dominant pole with a reduced single-particle strength and many other poles with rather small strength. The dominant pole is shifted in the direction of the Fermi surface, i.e. the level density at the Fermi surface is increased. The effective mass derived from this level

density in the Pb region is considerably increased, but there is still room for an additional energy dependence of the self-energy not taken into account by the coupling to surface vibrations. In addition we discussed several solutions of the response equations for nuclei in an external field. This allows to calculate the strength functions with respect to an external operator and the photo absorption cross sections in the correlated system. If one takes into account only the static part of the interaction one finds the usual RPA or QRPA results of time-dependent density functional theory, which reproduces the position of the resonances rather well, but it cannot account for the width that has its origin in the coupling to more complicated configurations. The energy-dependent part of the interaction includes this coupling and therefore it induces again a fragmentation of the rather sharp resonance peaks in RPA or QRPA over many complex configurations. Because of the subtraction procedure the position of the resonances is not changed very much, but the width is considerably increased, in excellent agreement with experimental data.

Of course there is room for additional improvements. So far, for numerical simplicity, exist only applications of this theory with the parameter set NL3, which has no density dependence in the isovector channel. At present there exist more modern parameter sets with the density dependent meson exchange [84, 85] which give already on the mean field level improved results for characteristic properties such as the neutron skin of neutron-rich nuclei or the density dependence of the symmetry energy. They should also be implemented in the theoretical investigations of the type discussed in this article. A further improvement can be achieved by using a more realistic pairing force. So far there are only investigations available with a monopole pairing force. It is therefore highly desirable to implement in the pairing channel a density dependent zero range force or the finite range Gogny force. All the calculations presented here have been done in a discrete basis, i.e. in the spectral representation of the response equation and therefore the coupling to the continuum is not taken into account properly so far. This might have a strong influence on application to light nuclei and therefore relativistic continuum RPA should be extended to relativistic continuum QRPA and relativistic continuum QTBA. Finally, so far ground state correlations have been taken into account only on the RQRPA level. In the non-relativistic case there exist investigations going beyond this limitations. They should be extended also to the relativistic calculations.

### Acknowledgments

Valuable discussions with V. Tselyaev are gratefully acknowledged. This work has been supported in part by the Bundesministerium für Bildung und Forschung under project 06 MT 246 and

by the DFG cluster of excellence “Origin and Structure of the Universe”(www.universe-cluster.de). E.L. acknowledge financial support from the Hessian LOEWE initiative through the Helmholtz International Center for FAIR and the Russian Federal Agency of Education, project No. 2.1.1/4779.

- 
- [1] W. Kohn and L. J. Sham, Phys. Rev. **137**, A1697 (1965).
  - [2] J. Engel, Phys. Rev. **C75**, 014306 (2007).
  - [3] B. G. Giraud, Phys. Rev. **C77**, 014311 (2008).
  - [4] M. Bender, P.-H. Heenen, and P.-G. Reinhard, Rev. Mod. Phys. **75**, 121 (2003).
  - [5] P. Ring, Prog. Part. Nucl. Phys. **37**, 193 (1996).
  - [6] D. Vretenar, A. V. Afanasjev, G. A. Lalazissis, and P. Ring, Phys. Rep. **409**, 101 (2005).
  - [7] S. T. Belyaev, Nucl. Phys. **24**, 322 (1961).
  - [8] S. T. Belyaev, *Collective Excitations in Nuclei* (Gordon Breach, New York, 1968).
  - [9] P. Ring and P. Schuck, *The Nuclear Many-Body Problem* (Springer-Verlag, Heidelberg, 1980).
  - [10] J. G. Valatin, Phys. Rev. **122**, 1012 (1961).
  - [11] E. Litvinova, P. Ring, and V. I. Tselyaev, Phys. Rev. **C78**, 014312 (2008).
  - [12] T. Gonzales-Llarena, J. L. Egido, G. A. Lalazissis, and P. Ring, Phys. Lett. **B379**, 13 (1996).
  - [13] J. Boguta and A. R. Bodmer, Nucl. Phys. **A292**, 413 (1977).
  - [14] Y. K. Gambhir, P. Ring, and A. Thimet, Ann. Phys. (N.Y.) **198**, 132 (1990).
  - [15] G. A. Lalazissis, D. Vretenar, and P. Ring, Euro. Phys. J. **A22**, 37 (2004).
  - [16] G. A. Lalazissis, M. M. Sharma, P. Ring, and Y. K. Gambhir, Nucl. Phys. **A608**, 202 (1996).
  - [17] J. Meng and P. Ring, Phys. Rev. Lett. **77**, 3963 (1996).
  - [18] G. A. Lalazissis, D. Vretenar, and P. Ring, Phys. Rev. **C69**, 017301 (2004).
  - [19] G. A. Lalazissis, D. Vretenar, and P. Ring, Nucl. Phys. **A650**, 133 (1999).
  - [20] A. V. Afanasjev, J. König, P. Ring, J. L. Egido, and L. M. Robledo, Phys. Rev. **C62**, 054306 (2000).
  - [21] A. V. Afanasjev, P. Ring, and J. König, Nucl. Phys. **A676**, 196 (2000).
  - [22] Z.-Y. Ma, A. Wandelt, N. Van Giai, D. Vretenar, P. Ring, and L.-G. Cao, Nucl. Phys. **A703**, 222 (2002).
  - [23] D. Vretenar, H. Berghammer, and P. Ring, Nucl. Phys. **A581**, 679 (1995).
  - [24] P. Ring, Z.-Y. Ma, N. Van Giai, D. Vretenar, A. Wandelt, and L.-G. Cao, Nucl. Phys. **A694**, 249 (2001).
  - [25] N. Paar, P. Ring, T. Nikšić, and D. Vretenar, Phys. Rev. **C67**, 034312 (2003).
  - [26] A. Ansari, Phys. Lett. **B623**, 37 (2005).
  - [27] J. P. Jeukenne, A. Lejeune, and C. Mahaux, Physics Reports **25**, 83 (1976).
  - [28] T. Nikšić, D. Vretenar, and P. Ring, Phys. Rev. **C73**, 034308 (2006).
  - [29] T. Nikšić, D. Vretenar, and P. Ring, Phys. Rev. **C74**, 064309 (2006).



- [30] L. D. Landau, Sov. Phys. JETP **8**, 70 (1959).
- [31] A. B. Migdal, *Theory of Finite Fermi Systems: Applications to Atomic Nuclei* (Wilson Interscience, New York, 1967).
- [32] P. Ring and J. Speth, Nucl. Phys. **A235**, 315 (1974).
- [33] P. Hohenberg and W. Kohn, Phys. Rev. **136**, B864 (1964).
- [34] P. Ring and E. Werner, Nucl. Phys. **A211**, 198 (1973).
- [35] I. Hamamoto and P. J. Siemens, Nucl. Phys. **A269**, 199 (1976).
- [36] A. Bohr and B. Mottelson, *Nuclear Structure* (Benjamin, Reading, Mass., 1975), Vol. II.
- [37] P. F. Bortignon, R. A. Broglia, D. R. Bes, and R. J. Liotta, Phys. Rep. **30C**, 305 (1977).
- [38] G. F. Bertsch, P. F. Bortignon, and R. A. Broglia, Rev. Mod. Phys. **55**, 287 (1983).
- [39] G. F. Bertsch, P. F. Bortignon, R. A. Broglia, and C. H. Dasso, Phys. Lett. **B80**, 161 (1979).
- [40] P. F. Bortignon and R. A. Broglia, Nucl. Phys. **A371**, 405 (1981).
- [41] G. Coló, P. F. Bortignon, N. Van Giai, A. Bracco, and R. Broglia, Phys. Lett. **B276**, 279 (1992).
- [42] G. Coló and P. F. Bortignon, Nucl. Phys. **A696**, 427 (2001).
- [43] D. Sarchi, P. F. Bortignon, and G. Coló, Phys. Lett. **B601**, 27 (2004).
- [44] V. I. Tselyaev, Sov. J. Nucl. Phys. **50**, 780 (1989); Yad. Fiz. **50**, 1252 (1989).
- [45] S. P. Kamerdzhiev, G. Y. Tertychny, and V. I. Tselyaev, Phys. Part. Nucl. **28**, 134 (1997).
- [46] S. P. Kamerdzhiev, J. Speth, and G. Y. Tertychny, Phys. Rep. **393**, 1 (2004).
- [47] V. I. Tselyaev, Phys. Rev. **C75**, 024306 (2007); arXiv:nucl-ph/0505031.
- [48] E. Litvinova and V. I. Tselyaev, Phys. Rev. **C75**, 054318 (2007); arXiv:nucl-ph/0512030.
- [49] V. G. Soloviev, *Theory of Atomic Nuclei: Quasiparticles and Phonons* (Institute of Physics, Bristol and Philadelphia, USA, 1992), textbook on QPM.
- [50] S. Drożdż, S. Nishizaki, J. Speth, and J. Wambach, Phys. Rep. **197**, 1 (1990).
- [51] E. Litvinova and P. Ring, Phys. Rev. **C73**, 044328 (2006).
- [52] E. Litvinova, P. Ring, and V. I. Tselyaev, Phys. Rev. **C75**, 064308 (2007).
- [53] E. Litvinova, P. Ring, V. I. Tselyaev, and K. Langanke, Phys. Rev. **C**, to be published (2009).
- [54] V. A. Khodel and E. E. Saperstein, Nucl. Phys. **A317**, 424 (1979).
- [55] V. A. Khodel and E. E. Saperstein, Nucl. Phys. **A348**, 261 (1980).
- [56] S. A. Fayans, S. V. Tolokonnikov, E. L. Trykov, and D. Zawischa, Nucl. Phys. **A676**, 49 (2000).
- [57] B. D. Serot and J. D. Walecka, Adv. Nucl. Phys. **16**, 1 (1986).
- [58] B. D. Serot and J. D. Walecka, Int. J. Mod. Phys. **E6**, 515 (1997).
- [59] P.-G. Reinhard, Rep. Prog. Phys. **52**, 439 (1989).
- [60] B. D. Serot, Rep. Prog. Phys. **55**, 1855 (1992).
- [61] A. R. Bodmer, Nucl. Phys. **A526**, 703 (1991).
- [62] Y. Sugahara and H. Toki, Nucl. Phys. **A579**, 557 (1994).
- [63] M. M. Sharma, A. R. Farhan, and S. Mythili, Phys. Rev. **C61**, 054306 (2000).
- [64] C. J. Horowitz and J. Piekarewicz, Phys. Rev. **C64**, 062802 (2001).

- [65] P. Manakos and T. Mannel, Z. Phys. **A334**, 481 (1989).
- [66] T. Bürvenich, D. G. Madland, J. A. Maruhn, and P.-G. Reinhard, Phys. Rev. **C65**, 044308 (2002).
- [67] T. Nikšić, D. Vretenar, G. A. Lalazissis, and P. Ring, Phys. Rev. **C78**, 034318 (2008).
- [68] W. Kohn, Rev. Mod. Phys. **71**, 1253 (1999).
- [69] R. M. Dreizler and E. K. U. Gross, *Density functional theory* (Springer, Berlin, Heidelberg, New York, 1990), textbook on DFT in electronic systems.
- [70] S. P. Kamerdzhiev and V. I. Tselyaev, Sov. J. Nuc. Phys. **44**, 214,392 (1986).
- [71] G. A. Lalazissis, J. König, and P. Ring, Phys. Rev. **C55**, 540 (1997).
- [72] G. A. Lalazissis, S. Raman, and P. Ring, Atomic and Nuclear Data Tables **71**, 1 (1999).
- [73] G. A. Lalazissis, S. Karatzikos, R. Fossion, D. P. Arteaga, A. V. Afanasjev, and P. Ring, Phys. Lett. **B671**, 36 (2009).
- [74] M. Jaminon and C. Mahaux, Phys. Rev. **C40**, 354 (1989).
- [75] M. Jaminon and C. Mahaux, Phys. Rev. **C41**, 697 (1990).
- [76] D. Vretenar, T. Nikšić, and P. Ring, Phys. Rev. **C65**, 024321 (2002).
- [77] A. P. Platonov, Sov. J. Nucl. Phys. **34**, 612 (1981).
- [78] R. P. J. Perazzo, S. L. Reich, and H. M. Sofia, Nucl. Phys. **A339**, 23 (1980).
- [79] V. Bernard and N. Van Giai, Nucl. Phys. **A348**, 75 (1980).
- [80] E. Litvinova, P. Ring, and D. Vretenar, Phys. Lett. **B647**, 111 (2007).
- [81] S. Shlomo and D. Youngblood, Phys. Rev. **C47**, 529 (1993).
- [82] Reference Input Parameter Library, Version 2, <http://www-nds.iaea.org/RIPL-2/>.
- [83] P. Adrich *et al*, Phys. Rev. Lett. **95**, 132501 (2005).
- [84] T. Nikšić, D. Vretenar, P. Finelli, and P. Ring, Phys. Rev. **C66**, 024306 (2002).
- [85] G. A. Lalazissis, T. Nikšić, D. Vretenar, and P. Ring, Phys. Rev. **C71**, 024312 (2005).
- [86] L. P. Gor'kov, Sov. Phys. JETP **34**, 505 (1958).
- [87] W. Brenig and H. Wagner, Z. Phys. **173**, 484 (1963).
- [88] P. Ring, L. M. Robledo, J. L. Egido, and M. Faber, Nucl. Phys. **A419**, 261 (1984).
- [89] J.-P. Blaizot and G. Ripka, *Quantum Theory of Finite Systems* (MIT Press, Cambridge, 1986).
- [90] Experimental Nuclear Reaction Data, <http://www-nds.iaea.or.at/exfor/exfor00.htm>.
- [91] A. Ansari and P. Ring, Phys. Rev. **C74**, 054313 (2006).